Available online at www.sciencedirect.com

jmr&t Journal of Materials Research and Technology

journal homepage: www.elsevier.com/locate/jmrt

Original Article

# Microstructural, mechanical and electrochemical properties of AlCrFeCuNiW$_x$ high entropy alloys

N. Malatji [a,*], T. Lengopeng [b], S. Pityana [b], A.P.I. Popoola [a]

[a] Tshwane University of Technology, Pretoria, South Africa
[b] Council for Scientific and Industrial Research, Pretoria, South Africa

ARTICLE INFO

*Article history:*
Received 7 October 2020
Accepted 25 January 2021
Available online 2 February 2021

*Keywords:*
High Entropy Alloys
Microstructure
Microhardness
Wear resistance
Corrosion behavior
Compressive properties

ABSTRACT

AlCrFeNiCuW$_x$ high entropy alloys were fabricated on 316 L stainless steel substrate using laser metal deposition technique. The microstructural and mechanical characteristics of these alloys were studied by advanced characterization techniques. The results revealed that the alloys exhibited a dual phase structure with BCC (body centered cubic) and FCC (face centered cubic) solid solution phases. The presence of tungsten (W) particles in the HEA matrix changed the shape of grains from columnar to aquiaxed. The alloys that contained W possessed higher plasticity at maximum compressive stress. They also showed better performance when they were evaluated for wear and corrosion.



## 1. Introduction

The excellent properties exhibited by high entropy alloys (HEAs) in different environments give them an urge over traditional alloys in applications where high performance is required. These alloys are characterized by high resistance to mechanical deformation and chemical degradation. They also maintain their integrity at high temperatures due to their good resistance to softening, oxidation and radiation [1–3]. The design of these alloys deviate from conventional routes where an alloy is composed of one or two major elements and some minor elements. The alloys are made up of five or more major elements in near/equal atomic proportions with high configurational entropy. They form simple solid solutions that are stable even in higher temperatures [4,5]. Amongst high entropy alloys, Al$_x$CoCrFeNi ($x \leq 1$) HEA$_s$ are some of the most promising alloys that can be used for structural applications [6]. They have been reported to possess dual phase structures and have presented exceptional properties such as high mechanical strength, good oxidation, corrosion and wear resistance [7–10]. Even though the presence of Co in the alloys improves its strength and ductility, this metal is highly expensive and pose practical problems for their adoption in industrial applications [11–13]. To reduce the use of cost intensive alloying elements, Co was replaced by Cu to produce novel Co-free Al$_x$CrCuFeNi HEAs. Cu forms a separate Cu-rich FCC phase since this element has positive mixing enthalpy with the other elements [14–16]. The formation of phases was also found to be dependent mainly on the content of Al

* Corresponding author.
E-mail address: doublen.malatji@gmail.com (N. Malatji).
https://doi.org/10.1016/j.jmrt.2021.01.103

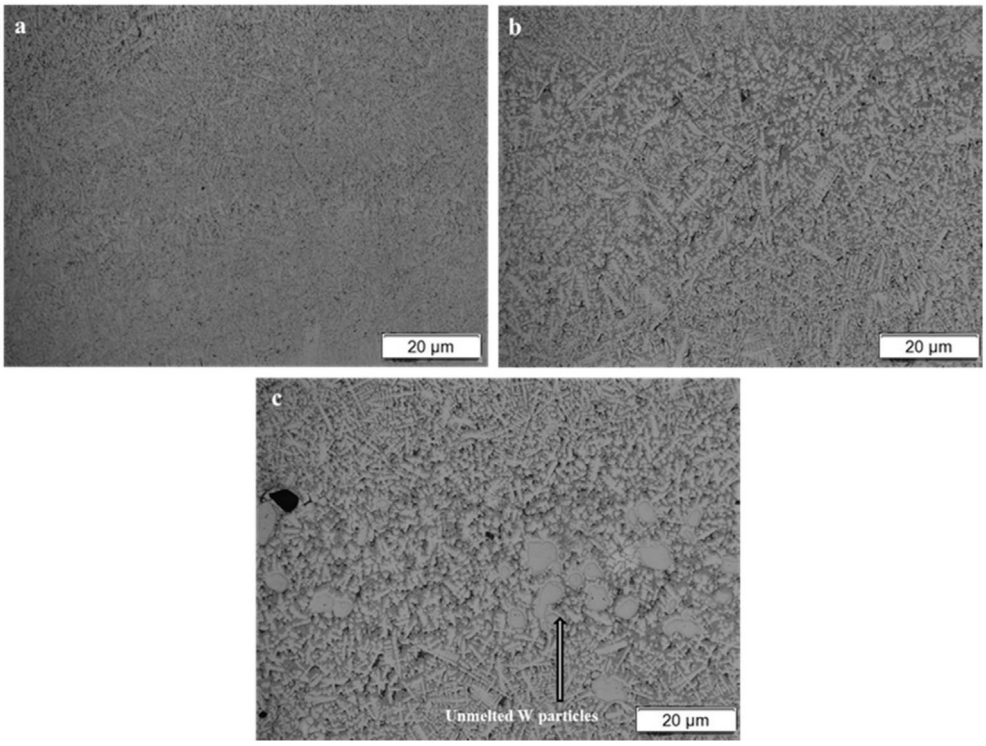


**Fig. 1 – OM Micrographs of AlCrFeNiCu HEA doped with W (a) without W, (b) 1 at.% W and (c) 3 at.% W.**

present in these alloys. High Al content favored formation of rich BCC phase structures while alloys with lower content of Al were found to be dominated by FCC ones [17,18]. Since alloys that have high proportion of BCC over FCC phase have high strength and low ductility, $Al_xCrCuFeNi$ HEAs with high content of Al requires modification of their microstructures to

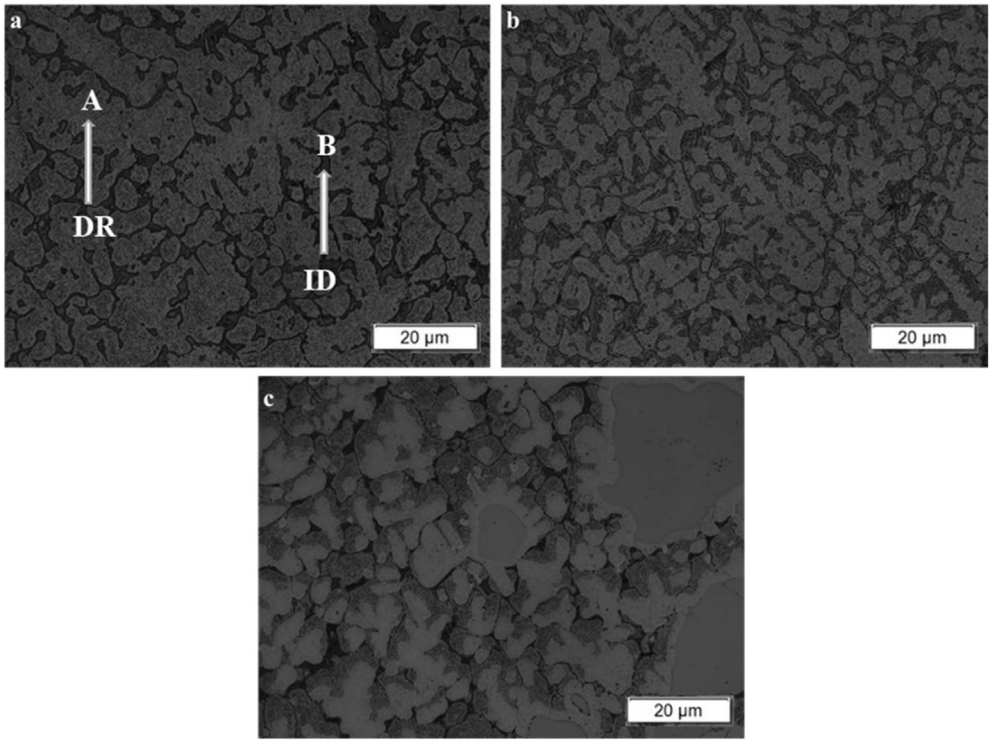


**Fig. 2 – OM Micrographs of $AlCrFeNiCuW_x$ (a) Without W, (b) 1 at.% W and (c) 3 at.% W; DR – dendritic and ID – interdendritic regions.**

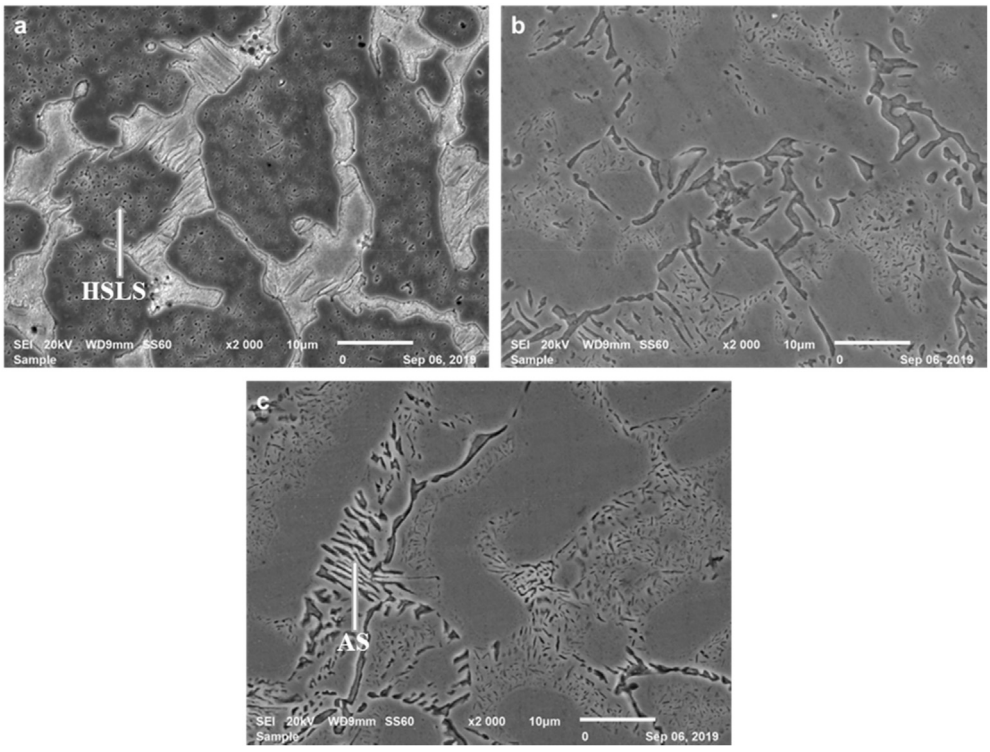


**Fig. 3 – SEM Micrographs of AlCrFeNiCu HEA doped with W (a) without W, (b) 1 at.% W and (c) 3 at.% W; HSLS – honeycomb sponge-like structures and AS – Acicular structures.**

improve their mechanical performance. One of the most effective ways to modify mechanical properties of HEAs is alloying. Incorporation of alloying elements into HEA matrices either induce solid solution strengthening or trigger formation of intermetallic phases [19–22]. Ma et al. [23] studied the effect of Nb addition on the microstructural and mechanical properties of AlCoCrFeNi HEA. The presence of Nb in the alloy promoted the formation of a laves phase and refinement of grains. The compressive yield strength was significantly improved while the ductility of the alloy was compromised. Similar results were obtained when Zr was incorporated into the same alloy [24]. The microstructure of the alloy was characterized by a laves phase and its volume fraction was dependent on the content of Zr in the alloy. On the other hand, addition of tungsten (W) into $CrFeNiV_{0.5}$ and $CrFeNi_2V_{0.5}$ HEA matrices proved to be beneficial for the compressive strength and ductility of these alloys [25]. The alloys were characterized of both strong BCC phase and ductile FCC and σ phases. Doping of AlCuCrFeMn HEA with W was reported to improve this alloy's electrochemical behavior [26]. Alloys which contained W exhibited higher corrosion resistance than the matrix alloy. Due to the positive influence of W on the microstructure of HEA matrixes, this alloying element was chosen to reinforce functional properties of AlCrFeCuNi HEAs in the current study. Its effect on the microstructural evolution, mechanical and electrochemical performance of AlCrFeCuNi HEAs was investigated.

## 2. Materials and methods

### 2.1. *Material preparation*

$AlCrFeNiCuW_x$ (x = 1 and 3 at%) high entropy alloys were prepared by laser metal deposition technique. A blend of high purity metallic powders [supplied by WEARTECH (PTY) LTD, purity >99.5 wt. %, size varying from 90 to 150 μm] of Al, Cr, Fe, Ni, Cu and W mixed together in a tubular mixer for 48 h was used as a feedstock material for deposition. A 5 kW $CO_2$ laser was then used to produce the HEA deposits on a 6 mm thick sand blasted and heated 316 stainless steel (supplied by MACSTEEL) substrate. Constant laser power of 1600 W, scanning speed of 1.2 m/min and substrate heating temperature of 400 °C were used during the production of the alloys. The deposits were built under argon environment (1.5–1.8 L/min) while keeping individual layer thickness at 0.04 mm and overlapping ratio at 50%. Multi-directional scanning strategy was used and a final deposit with dimensions of 30 × 30 × 10 mm was achieved.

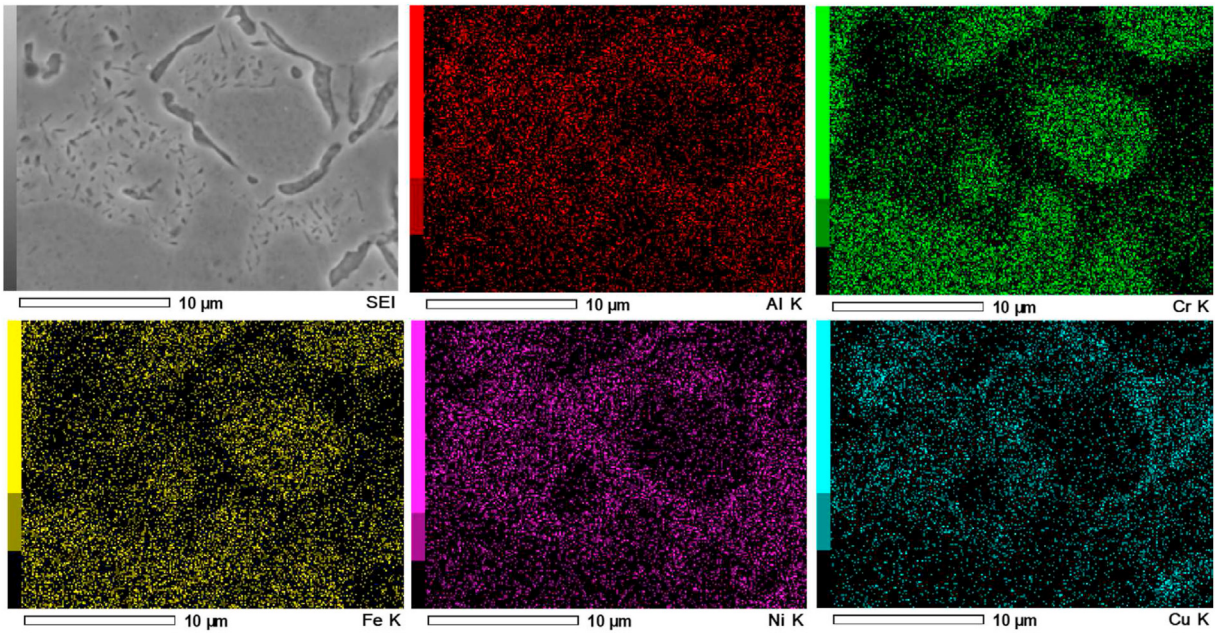


**Fig. 4 – EDS mapping of AlCrFeNiFeCu HEA doped with 1 at.% W.**

### 2.2. *Microstructural and morphological characterization*

Metallographic samples were sectioned using an EDM wire cutter. The samples were mounted, polished and etched with aqua-regia solution. Analysis of the microstructure and chemical composition of the alloys was carried out using JEOL JSM-6010PLUS/LA scanning electron microscope (SEM) equipped with energy dispersive spectrometer (EDS). Phase analysis was conducted using D/Max-2200 PC X-ray diffractometer with Cu Kα diffraction generated at 40 kV and 45 mA. Scan rate of 1°/min was used to obtain the diffractograms and High Score software was used to identify the phases that have formed.

### 2.3. *Mechanical testing*

Hardness measurements across the specimen surfaces were performed using the Emco Test Durascan microhardness tester. A load of 300 gf with retention time of 15 s was used at ten different points and the average was recorded.

Rtec ball on disk tribometer was used evaluate the friction and wear characteristics of the alloy. The wear specimen were sectioned to be 10 × 5 × 5 mm. Silicon carbide ball was used as a wear medium and the time duration for the test was 8 min. A normal load of 150 N at sliding velocity of 2 mm/s and distance of 3 mm was applied during the test. The mass of the samples were recorded prior and post wear experiments to determine the wear loss.

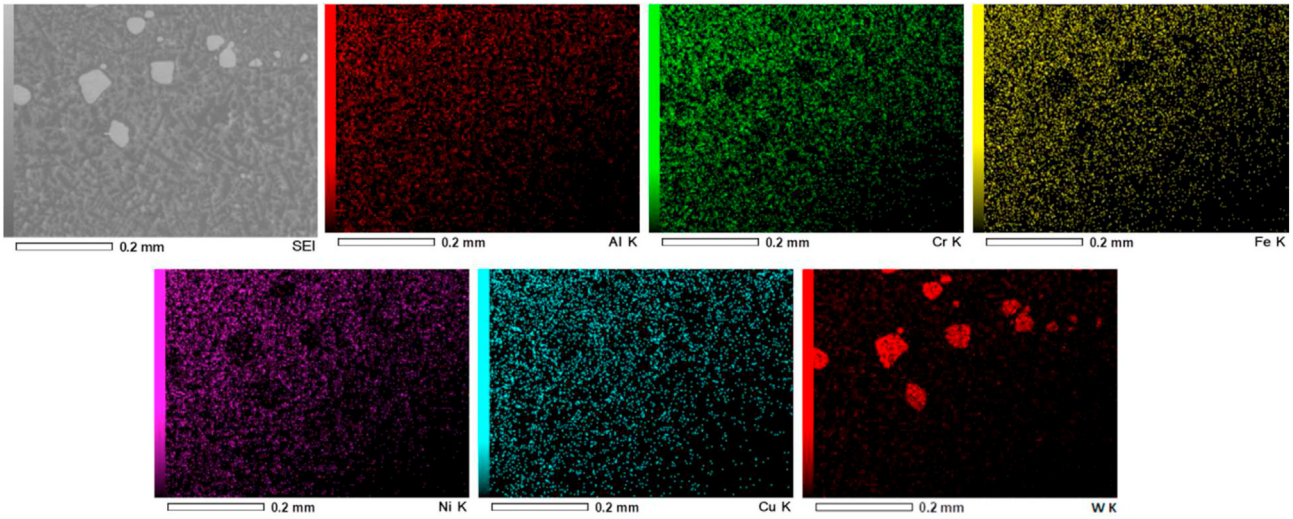


**Fig. 5 – EDS mapping of AlCrFeNiCu HEA doped with 3 at% W.**

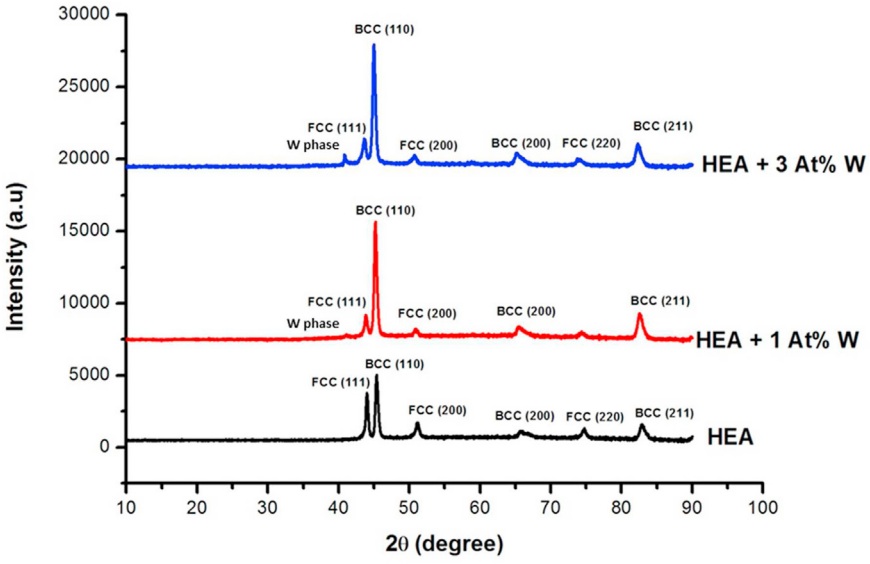


**Fig. 6 – XRD patterns of AlCrFeNiCuW$_x$ HEAs.**

Instron 1175 machine was used to measure the compressive stress and strain of the alloys. Rectangular specimen with dimensions of 5 × 5 mm$^2$ cross section and height of 10 mm were used during compressive testing. The samples were compressed using a strain rate of 0.033 mm/s.

### 2.4. *Electrochemical behavior*

Potentiodynamic polarization technique was used to investigate the corrosion resistance of the HEAs in 0.5 M $H_2SO_4$ solution using μAUTOLAB Pontentiostat/Galvanostat. The polarization measurements were carried from a potential of −1.5 to 1.5 V with a scanning rate of 0.01 V/s. Saturated calomel electrode was used as a reference and platinum served as a counter electrode. The HEA samples were used as working electrode with an exposed area of 1 cm$^2$. Nova 1.8 was used to extrapolate the corrosion parameters obtained from the Tafel curves.

## 3. Results and discussion

### 3.1. *Microstructural analysis*

Figs. 1 and 2 show the optical micrographs of AlCrFeNiCu HEA reinforced with 1–3 at% of W obtained at different magnifications. A dendritic microstructure with dendritic (DR) and interdendritic (ID) regions is prevalent in all the alloys. However, alloys containing W shows the presence of some partially melted particles in some regions of the deposit. The partially melted particles were assumed to be W since it has high melting point of around 3 300 °C. Similar results were obtained in HEAs that contained W and fabricated using laser additive manufacturing [27]. Some white large-sized W particles were found to be partially melted in MoFeCrTiWAlNb refractory HEA coating even though the laser power that was used was two times higher than the one employed in this work.

EDS maps shown in Fig. 5 confirmed that the particles are composed of 100% W. The particles were noticed to segregate along the bottom of each layer of the build. The high density associated with W may be responsible for the manner in which they are segregated. The density of W is more than twice that of Cu and Ni, which are the heaviest elements in the un-reinforced alloy. Variation in morphological characteristics was also observed around the areas with high density of W in the HEA containing 3 at% W (see Figs. 1c and 2c). The dendrites around these areas are aquiaxed while those that are away have a columnar structure. Presence of dispersed particles during crystallization have been reported to enhance nucleation rate and cause a change in shape and size of grains [28]. The

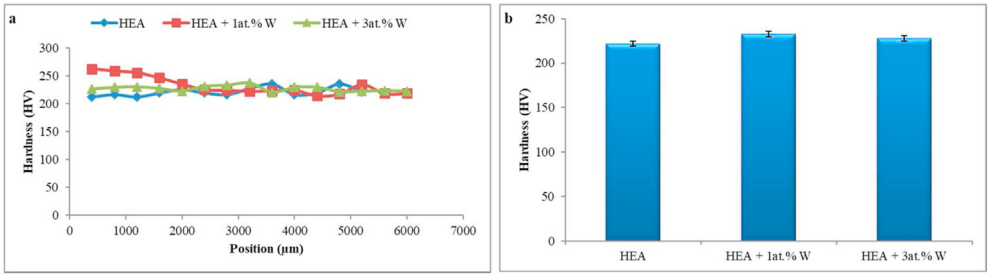


**Fig. 7 – Microhardness values of AlCrFeNiCuW$_x$ HEAs (a) profile and (b) average.**

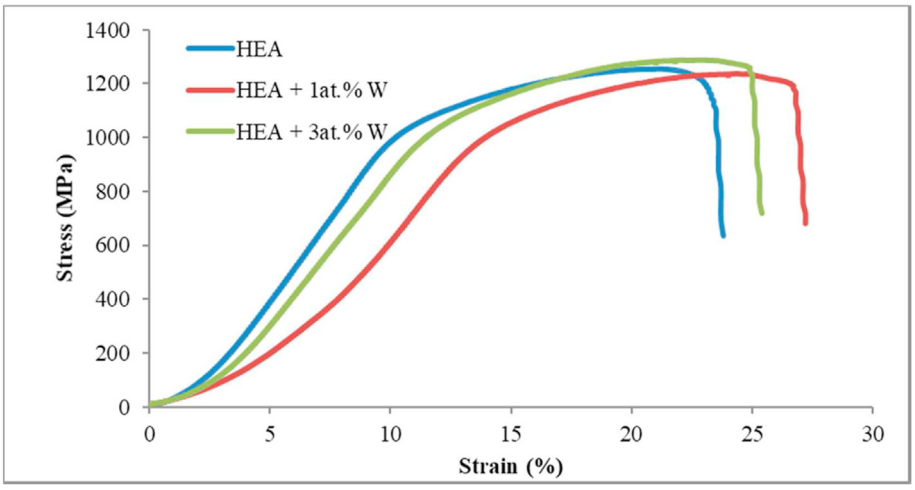


**Fig. 8 – Compressive stress vs strain for AlCrFeNiCuW$_x$ HEAs.**

particles act as heterogeneous nuclei and prevents formation of columnar grains. According to Chang et al. [29], the much higher atomic radius associated with W as compared to the other HEA matrix components causes variations in potential energies of lattice sites and lowers the diffusion rates.

Fig. 2 also reveals that the HEA matrix is composed of mainly two phase regions (separate from each other) marked A and B. Each region is composed of two phases that are dark and light grey in color. Region A consist of two phase structure (BCC and FCC phases) while a one phase structure is predominant in region B (BCC phase). An enlargement of an area containing BCC phase occurs as result of adding W into the matrix. The structure exhibited by the alloys is similar to those obtained from casting techniques [23,24].

Fig. 3 shows the SEM images of AlCrFeNiCuW$_x$ HEAs. The structure shown by these images corresponds to those revealed by optical micrographs. The DR region contains honeycomb sponge-like structure (HSLS) while acicular structures (AS) are found in the ID region. The area of the acicular' structures grows as the content of W is increased. EDS maps in Fig. 4 show the distribution of elements within the microstructure. The honeycomb sponge like structures are rich in Fe and Cr. On the other hand, the acicular structures consist of two phases, one enriched with Al and Ni while the other one contains Cu rich phase. According to literature [7–12], Fe–Cr and Al–Ni are BCC phases and Cu rich one is FCC phase. The results are supported by X-ray diffractions patterns shown in Fig. 6. The intensities of FCC phase are reduced while that of BCC is increased. A new peak is observed at 2θ of 41° for alloys containing W. The peak corresponds with formation of W phase.

**Table 1 – Compressive yield stress, maximum stress and strain of AlCrFeNiCuW$_x$ HEAs.**

| Alloy | Yield Stress (MPa) | Maximum Stress (MPa) | Strain (%) |
|---|---|---|---|
| HEA | 1010.5 | 1253.92 | 21.3 |
| HEA + 1 at.% W | 998.4 | 1274.6 | 24.3 |
| HEA + 3 at.% W | 1005.9 | 1287.9 | 23.4 |

### 3.2. *Microhardness property*

Fig. 7 shows the profile and average microhardness values obtained from AlCrFeNiCuW$_x$ HEAs. Uniform microhardness profile was observed for HEA matrix and HEA containing 3 at% of W. The HEA with 1 at% of W had higher microhardness values at the top of the deposit and became uniform in the middle and bottoms regions of the deposit. Irregularity of distribution of W particles in alloy containing 1 at. % W was found to be higher than the one with 3 at. % of W. Since these particles served as heterogeneous nuclei, the formation of aquiaxed grains was also irregular. This caused the upper region of the deposit to have a different microstructure as compared to the middle and bottom regions. Despite the alloys with 1 and 3 at% of W possessing higher average microhardness values than the HEA matrix, the difference was lower than 20 HV which is considered to be negligible. Pure single-crystalline W has high ductility and its incorporation in the matrix in very low concentrations may not have significant influence on the hardness of the alloy.

### 3.3. *Compressive properties*

Compressive tests were used to study the bulk mechanical properties of the alloys. Fig. 8 shows the compressive stress and strain curves of AlCrFeNiCuW$_x$ HEAs. The values of the yield stress, maximum compressive stress and strain at maximum stress are shown in Table 1. The un-doped alloy possesses yield stress of 1010.5 MPa, maximum stress of 1253.92 MPa and strain at maximum stress of 21.3%. Introduction of W into the HEA matrix caused a positive shift in strain at yield and maximum stress. An improvement of 2.1% and 3% in strain at maximum compressive stress were obtained for alloys with 1 at. % and 3 at. % W, respectively. While

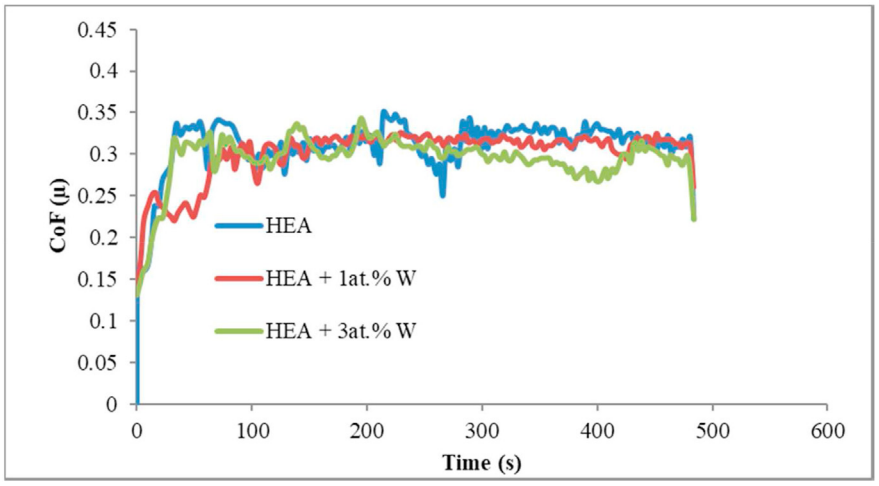


**Fig. 9 – Friction behavior of AlCrFeNiCuW$_x$ HEAs.**

no improvement in yield stress was recorded for all contents of W addition, the difference in yield stress values of all the alloys was lower than 10 MPa. An increase of around 21 and 34 MPa in maximum compressive stress were achieved when 1 at. % and 3 at. % of W was incorporated into the HEA matrix, respectively. The improvement in compressive properties of AlCrFeNiCuW$_x$ HEAs can be attributed to the inclusion of W in the matrix of the HEA. The presence of W particles in the melt pool changed the solidification dynamics of the HEA matrix. These particles act as heterogeneous nuclei and promote a transition in the shape of grains from columnar to aquiaxed [28]. The shape of grains changes the grain aspect ratio, length to diameter, which have significant effect on the behavior of a material during deformation. According to Rathmayr et al. [30], low grain aspect ratio increases average shear stress on the grain boundaries and allows higher degree of grain boundary sliding. This causes the strength of the material to decrease while its ductility is improved. However, in this work, the mixture of grain aspect ratios, exhibited by columnar and aquiaxed grains in alloys containing W, makes it possible for them to retain their strength while their ductility is improved. As it has been discussed under EDS results, the Cu-rich phase content reduces with increase in the amount of W added. The reduction of this phase increased the amount of acicular structures, which have positive effect on the strength and ductility of the alloys.

Wetting of un-melted W particles may also be attributed to the reduction in ductility. Un-wetting of these particles reduces the binding strength between the matrix and the W phase [31]. Higher content and irregular distribution of W in alloy containing 3 at. % of W increase the un-wettability of W and reduce the binding strength. Therefore, areas of the deposit with agglomerated and un-wetted W particles serve as weak site for failure during stressing. The lines of the curves are smooth in the toe, elastic and plastic regions except upon fracture. This implies that no cracking of the samples occurs until fracture.

### 3.4. *Tribological properties*

Friction behavior of AlCrFeNiCuW$_x$ HEAs is shown in Fig. 9. High increase of coefficient of friction (CoF) values is observed

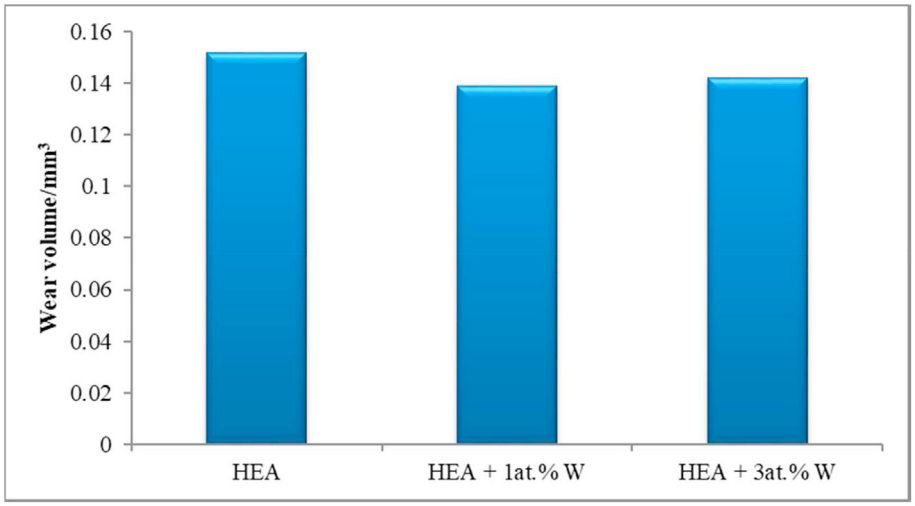


**Fig. 10 – Wear volume of AlCrFeNiCuW$_x$ HEAs.**

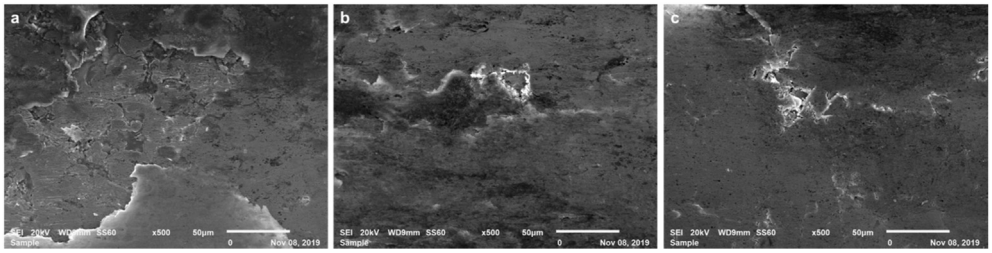


**Fig. 11 – Worn out surfaces of AlCrFeNiCuW$_x$ HEAs.**

for the first 100 s for all the alloys. The un-doped alloy showed the highest CoF value of around 0.34 during this time. As the test progresses, the CoF values of this alloy stabilizes but spikes in the value of CoF were noticed between 200 and 280s. Alloys that contains W possess slightly lower CoF values and fluctuations of these values are minimal throughout the test. The friction behavior of the alloys in the first 100s is consistent with rough contact between the surface of the alloy and silicon carbide ball. The resistance of the alloy to wear is high during initial contact and decreases with time of exposure to wear. During wear, debris are generated and adhere to the surface. The adhered wear debris reduce the contact between the surface of the alloy and wear medium. This leads to reduction in CoF values and wear rate of the alloy. The stabilization of the CoF values is dependent on the retention of the adhered debris on the wear track. The longer these materials are present on the wear track, the lower the fluctuation in CoF values. The opposite is true when the wear debris are retained for shorter times on the wear track. Another factor that has been reported to reduce friction during wear is the formation of oxide film on the wear surface. The increase of temperature due to friction heat accumulation creates a conducive environment for oxides to form as a result of interaction between oxygen from air and metallic elements in the alloy [32]. The adherence of the oxide film to the surface of the alloy and counterpart reduce the amount of friction generated.

Fig. 10 shows the wear volume of AlCrFeNiCuW$_x$ HEAs. The un-doped HEA exhibited the highest wear volume of 0.152 mm$^3$. Incorporation of 1 at. % and 3 at. % of W into the HEA matrix decreased the wear volume to 0.139 and 0.142 mm$^3$, respectively. Despite the slight difference in wear volume between the alloy containing 1 at. % and 3 at. % of W, presence of W in HEA matrix improved its wear resistance. Irregularity in distribution of W in the HEA matrix may be attributed to this behavior. The change in wear volume is in harmony with the microhardness property exhibited by the alloys. To understand the nature and effect of wear experienced by the alloys, worn surfaces were characterized by SEM. The worn morphologies of AlCrFeNiCuW$_x$ HEAs are shown in Fig. 11. Severe surface damage is visible on the alloy with no presence of W. The damaged is caused mainly by surface peeling, grooving and scratching. However, the degree of the damage was reduced when W was introduced into the HEA matrix. The wear tracks of these alloys were shallower and had minimal delamination. According to Yu et al. [20], the resistance of a material to plastic deformation during wear is mainly dependent on its hardness property. The materials with higher hardness have higher resistance to deform plastically. Despite the alloys which contained some amount of W showing minor improvement in hardness, the slight increase in hardness of these alloys may change their surface characteristics.

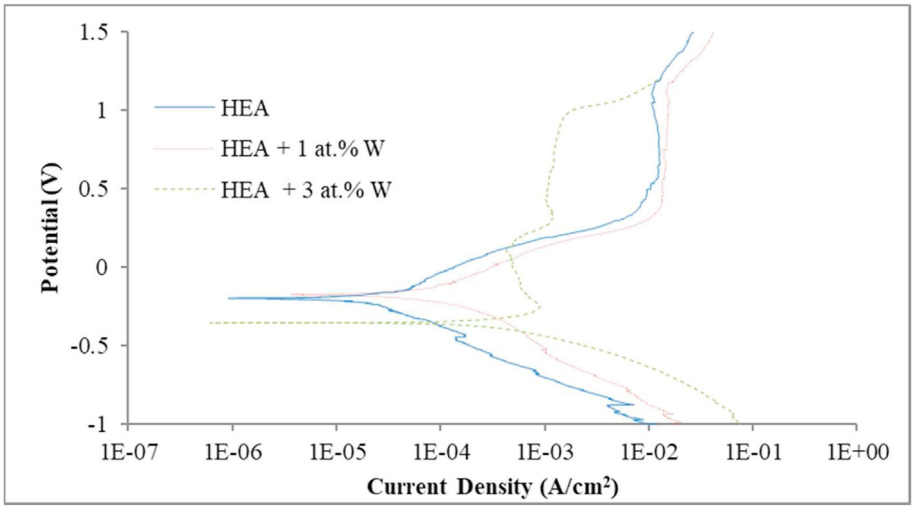


**Fig. 12 – Polarization curves of AlCrFeNiCuW$_x$ HEAs.**

**Table 2 – Electrochemical parameters of $AlCrFeNiCuW_x$ HEAs obtained from potentiodynamic polarization curves by linear fitting.**

| | $E_{corr}$ (V) | $I_{corr}$ (A/cm$^2$) | $R_p$ (Ω) | CR (mm/year) |
|---|---|---|---|---|
| HEA | −0.19936 | 2.99E−05 | 1284.5 | 0.34774 |
| HEA+1 at. % W | −0.1748 | 14.4E−05 | 572.95 | 1.6693 |
| HEA+3 at. % W | −0.3560 | 51.1E−05 | 89.66 | 5.9364 |

### 3.5. *Electrochemical characteristics*

Electrochemical behavior of $AlCrFeNiCuW_x$ HEAs was evaluated using linear polarization in 0.5 M $H_2SO_4$ solution. Linear polarization curves are shown in Fig. 12 while the Taffel plots parameters are presented in Table 2. The results reveal that the incorporation of 1 at. % of W into the HEA matrix does not have significant effect on its corrosion resistance. The HEA without the presence of W exhibited lowest current density than all the other alloys. The difference in corrosion potential between the HEA matrix and HEA containing 1 at. % of W was also very narrow. According to electrochemical theory, lower corrosion current density and higher potentials show superior resistance to corrosion [33,34]. It was observed that the HEA matrix starts to passivate at lower current density than HEA with 1 at. % W. However, the base alloy also showed some fluctuation in current density in the passive region, which indicates that the passivating layer formed is not stable enough. Since the passivating layer perturb further interaction between corrosive medium and the surface of the alloy, its breakage exposes fresh surfaces and worsen corrosion. Increasing the content of W from 1 at. % to 3 at. % proved to have positive influence on the passivation of AlCrFeNiCu HEA. The alloy started passivation at lower current density and had wider range of passive window. Moreover, the alloy start pitting at low current density and the difference in $E_{pit}$ values of all the alloys is small. $E_{pit}$ is the potential value where sudden increase in current occurs and indicates the beginning of pitting of the protective passive layer [35]. Therefore, the presence of W in higher content in the HEA matrix influences the electrochemical characteristics of the alloy. Similar results were reported by Chen et al. [24] when W was incorporated into AlCuCrFeMn HEA matrix. W forms an oxide layer in the outer region of the Cr passivating layer and acts as an inhibiting agent to pitting. The $WO_3$ layer also allows the $Cr_2O_3$ film to grow and to be stabilized.

## 4. Conclusion

In this study, $AlCrFeNiCuW_x$ HEAs were prepared by laser metal deposition technology. The microstructural, mechanical and electrochemical characteristics of these alloys were investigated. The following conclusions were made:

- Incorporation of W into AlCrFeNiCu HEA matrix stabilizes the BCC phase and promotes evolution of an aquiaxed microstructure.
- The addition of W improved the plasticity of the HEA. The strain at maximum compressive stress of the alloy was increased by 3% and 2.1% when 1 at% and 3 at% of W were added, respectively.
- The presence of W in the HEA matrix enhanced the wear performance of the alloy. Alloys that contained amount of W possessed lower volume loss than the HEA matrix. The wear scars of the reinforced alloys showed less surface damage as compared to the matrix alloy.

## Author's contribution

All authors have participated in (a) conception and design, or analysis and interpretation of the data; (b) drafting the article or revising it critically for important intellectual content; and (c) approval of the final version.

## Declaration of Competing Interest

The authors declare that they have no known competing financial interests or personal relationships that could have appeared to influence the work reported in this paper.

## Acknowledgement

This work is based on the research supported by National Research Foundation of South Africa for the Grant, Unique Grant No. 120622. Research facilities were supported by Tshwane University of Technology and Council for Scientific and Industrial Research.

## REFERENCES

[1] Brechtl J, Chen S, Lee C, Shi Y, Feng R, Xie X, et al. A review of the serrated-flow phenomenon and its role in the deformation behavior of high-entropy alloys. Metals 2020;10(8):1101.
[2] Waseem OA, Ryu HJ. Combinatorial synthesis and analysis of AlxTayVz-Cr20Mo20Nb20Ti20Zr10 and Al10CrMoxNbTiZr10 refractory high-entropy alloys: oxidation behavior. J Alloys Compd 2020;828:154427.
[3] El-Atwani O, Li N, Li M, Devaraj A, Baldwin JKS, Schneider MM, et al. Outstanding radiation resistance of tungsten-based high-entropy alloys. Sci Adv 2019;5(3):9.
[4] Zhang Y, Zuo TT, Tang Z, Gao MC, Dahmen KA, Liaw PK, et al. Microstructures and properties of high-entropy alloys. Prog Mater Sci 2014;61:1–93.
[5] Lu Y, Dong Y, Guo S, Jiang L, Kang H, Wang T, et al. A promising new class of high-temperature alloys: eutectic high-entropy alloys. Sci Rep 2014;4:6200.
[6] Lu Y, Gao X, Jiang L, Chen Z, Wang T, Jie JC, et al. Directly cast bulk eutectic and near-eutectic high entropy alloys with balanced strength and ductility in a wide temperature range. Acta Mater 2016;124:143–50.
[7] Munitz A, Salhov S, Hayun S, Frage N. Heat treatment impacts on the micro-structure and mechanical properties of AlCoCrFeNi high entropy alloy. J Alloys Compd 2016;683:221–30.

[8] Chen L, Zhou Z, Tan Z, He D, Bobzin K, Zhao L, et al. High temperature oxidation behavior of $Al_{0.6}CrFeCoNi$ and $Al_{0.6}CrFeCoNiSi_{0.3}$ high entropy alloys. J Alloys Compd 2018;764:845–52.
[9] Liang J, Cheng K, Chen S. Effect of heat treatment the phase evolution and mechanical properties of atomized AlCoCrFeNi high-entropy alloy powders. J Alloys Compd 2019;803:484–90.
[10] Park JM, Moon J, Bae JW, Jung J, Lee S, Kim HS. Effect of annealing heat treatment on microstructural evolution and tensile behavior of $Al_{0.5}CoCrFeMnNi$ high-entropy alloy. Mater Sci Eng 2018;728:251–8.
[11] Guo S, Ng C, Liu CT. Anamalous solidification microstructures in Co-free $Al_xCrCuFeNi_2$ high-entropy alloys. J Alloys Compd 2013;557:77–81.
[12] Kang M, Lim KR, Won JW, Na YS. Effect of Co content on the mechanical properties of A2 and B2 phases in $AlCo_xCrFeNi$ high-entropy alloys. J Alloys Compd 2018;769:808–12.
[13] Wang X, Zhang Y, Ma X. High temperature deformation and dynamic recrystallization behavior of AlCrCuFeNi high entropy alloy. Mater Sci Eng 2020;778:139077.
[14] Jinhong P, Ye P, Hui Z, Lu Z. Microstructure and properties of AlCrFeCuNix ($0.6 \leq x \leq 1.4$) high-entropy alloys. Mater Sci Eng 2012;534:228–33.
[15] Guo L, Wu W, Ni S, Wang Z, Song M. Effects of annealing on the microstructural evolution and phase transition in an $AlCrCuFeNi_2$ high entropy alloy. Micron 2017;101:69–77.
[16] Verma A, Tarate P, Abhyankar AC, Mohape MR, Gowtam DS, Deshmukh VP, et al. High temperature wear in $CoCrFeNiCu_x$ high entropy alloys: the role of Cu. Scripta Mater 2019;161:28–31.
[17] Sistla HR, Newkirk JW, Liou FF. Effect of Al/Ni ratio, heat treatment on phase transformations and microstructure of $Al_xFeCoCrNi_{2-x}$(x= 0.3, 1) high entropy alloys. Mater Des 2015;81:113–21.
[18] Li M, Gasquez J, Boresevich A, Mishra R, Flores KM. Evaluation of microstructure and mechanical property variations in $Al_xCoCrFeNi$ high entropy alloys produced by a high-throughput laser deposition method. Intermetallics 2018;95:110–8.
[19] Ji W, Wang W, Wang H, Zhang J, Wang Y, Zhang F, et al. Alloying behavior and novel properties of CoCrFeNiMn high-entropy alloy fabricated by mechanical alloying and spark plasma sintering. Intermetallics 2015;56:24–7.
[20] Yu Y, He F, Qiao Z, Wang Z, Liu W, Yang J. Effects of temperature and microstructure on tribological properties of $CoCrFeNiNb_x$ eutectic high entropy alloys. J Alloys Compd 2019;775:1376–85.
[21] An Q, Wang J, Liu Y, Liu B, Guo W, Fang Q, et al. Effects of C and Mo on microstructures and mechanical properties of dual phase high entropy alloys. Intermetallics 2019;110:106471.
[22] Hou L, Hui J, Yao Y, Chen J, Liu J. Effects of Boron content on microstructure and mechanical properties of $AlFeCoNiB_x$ high entropy alloy prepared by vacuum arc melting. Vacuum 2019;164:212–8.
[23] Ma SG, Zhang Y. Effect of Nb addition on the microstructure and properties of AlCoCrFeNi high-entropy alloy. Mater Sci 2012;532:480–6.
[24] Chen J, Niu P, Liu Y, Lu Y, Wang X, Peng Y, et al. Effect of Zr content on microstructure and mechanical properties of AlCoCrFeNi high entropy alloy. Mater Des 2016;94:39–44.
[25] Jiang H, Han K, Lu Y, Wang T, Cao Z, Li T. Effects of tungsten on microstructure and mechanical properties of $CrFeNiV_{0.5}W_x$ and $CrFeNi_2V_{0.5}W_x$ high entropy alloys. J Eng Mater Perform 2015;24:4594–600.
[26] Kumar D, Maulik O, Sharma VK, Prasad YVSS, Kumar V. Understanding the effect of tungsten on the corrosion behavior of $AlCuCrFeMnW_x$ high-entropy alloys in 3.5 wt. % NaCl solution. J Mater Eng Perform 2018;27:4481–8.
[27] Guo Y, Liu Q. MoFeCrTiWAlNb refractory high-entropy alloy coating fabricated by rectangular-spot laser cladding. Intermetallics 2018;102:78–87.
[28] Bolzoni L, Xia M, NBabu NH. Formation of equiaxed crystal structures in directionally solidified Al-Si alloys using Nb-based heterogeneous nuclei. Sci Rep 2016;6:39554.
[29] Chang R, Fang W, Bai X, Xia C, Zhang X, Yu H, et al. Effects of tungsten additions on the microstructure and mechanical properties of CoCrNi medium entropy alloys. J Alloys Compd 2019;790:732–43.
[30] Rathmayr GB, Hehenwarter A, Pippan R. Influence of grain shape and orientation on the mechanical properties of high pressure torsion deformed nickel. Mater Sci Eng 2013;560:224–31.
[31] Kiran UR, Venkat S, Rishikesh B, Iyer VK, Sankaranarayana M, Nandy TK. Effect of tungsten content on microstructure and mechanical properties of swaged tungsten heavy alloys. Mater Sci Eng 2013;582:389–96.
[32] Juan YF, Li J, Jiang YQ, Jia WL, Lu ZJ. Modified criterions for phase prediction in the multi-component laser-clad coatings and investigations into microstructural evolution/wear resistance of $FeCrCoNiAlMo_x$ laser-clad coatings. Appl Surf Sci 2019;465:700–14.
[33] Qui X, Liu C. Microstructure and properties of $Al_2CrFeCoCuTiNi_x$ high-entropy alloys prepared by laser cladding. J Alloys Compd 2013;553:216–20.
[34] Qui Y, Thomas S, Fabajanic D, Barlow AJ, Fraser HL, Birbilis N. Microstructural evolution, electrochemical and corrosion properties of $Al_xCoCrFeNiTi_y$ high entropy alloys. Mater Des 2019;170:107698.
[35] Ye Q, Feng K, Li Z, Lu F, Li R, Huang J, et al. Microstructure and corrosion properties of CrMnFeCoNi high entropy alloy coating. Appl Surf Sci 2017;396:1420–6.